Integrated pan-Arctic melt onset detection from satellite active and passive microwave measurements, 2000–2009

L. Wang,[1] G. J. Wolken,[2,3] M. J. Sharp,[3] S. E. L. Howell,[1] C. Derksen,[1] R. D. Brown,[4] T. Markus,[5] and J. Cole[1]

Received 16 May 2011; revised 15 August 2011; accepted 31 August 2011; published 16 November 2011.

[1] An integrated pan-Arctic melt onset data set is generated for the first time by combining estimates derived from active and passive microwave satellite data using algorithms developed for the northern high-latitude land surface, ice caps, large lakes, and sea ice. The data set yields new insights into the spatial and temporal patterns of mean melt onset date (MMOD) and the associated geographic and topographic controls. For example, in the terrestrial Arctic, tree fraction and latitude explain more than 60% of the variance in MMOD, with the former exerting a stronger influence on MMOD than the latter. Elevation is also found to be an important factor controlling MMOD, with most of the Arctic exhibiting significant positive relationships between MMOD and elevation, with a mean value of 24.5 m d^{-1}. Melt onset progresses fastest over land areas of uniform cover or elevation (40–80 km d^{-1}) or both and slows down in mountainous areas, on ice caps, and in the forest-tundra ecotones. Over sea ice, melt onset advances very slowly in the marginal seas, while in the central Arctic the rate of advance can exceed 100 km d^{-1}. Comparison of the observed MMOD with simulated values from the third version of the Canadian Coupled Global Climate Model showed good agreement over land areas but weaker agreement over sea ice, particularly in the central Arctic, where simulated MMOD is about 2–3 weeks later than observed because of a cold bias in simulated surface air temperatures over sea ice.

Citation: Wang, L., G. J. Wolken, M. J. Sharp, S. E. L. Howell, C. Derksen, R. D. Brown, T. Markus, and J. Cole (2011), Integrated pan-Arctic melt onset detection from satellite active and passive microwave measurements, 2000–2009, *J. Geophys. Res.*, *116*, D22103, doi:10.1029/2011JD016256.

1. Introduction

[2] The increase in annual surface mean air temperature over the Arctic in recent decades has been almost twice as large as the global mean [*Trenberth et al.*, 2007]. The amplified warming is predominantly surface based in the spring period, consistent with positive feedbacks from decreasing snow and ice cover [*Screen and Simmonds*, 2010, 2011]. The primary temperature feedbacks are related to changes in surface albedo associated with the timing and duration of summer melt on all components of the cryosphere [*Déry and Brown*, 2007; *Groisman et al.*, 1994; *Perovich et al.*, 2007a, *Flanner et al.*, 2011]. Before the onset of spring melt, surface albedo is spatially uniform over much of the Arctic. During the melt season, however, there are considerable spatial and temporal variations in surface albedo across all elements of the cryosphere [*Grenfell and Perovich*, 2004]. The timing of terrestrial snowmelt coincides with the seasonal switch from the landscape being a net source to a net sink for atmospheric carbon, and it affects the length of the active growing season and the stability of permafrost [*Goulden et al.*, 1998; *Betts et al.*, 1998; *Myneni et al.*, 1997]. The total amount of solar energy absorbed by sea ice during the melt season is strongly related to the timing of melt onset [*Perovich et al.*, 2007a, 2007b]. Earlier melt onset allows for earlier development of melt ponds and open water areas that enhance the ice-albedo feedback and in turn contribute to sea ice reduction [*Stroeve et al.*, 2006]. On land ice, melt onset timing is closely related to melt season duration, which is a major influence on the interannual and longer term variability in the surface mass balance of high Arctic glaciers [*Koerner*, 2005; *Gardner and Sharp*, 2007; *Sharp and Wang*, 2009].

[3] Previous studies indicate that climate models have difficulties in accurately simulating the timing of spring snowmelt, and models exhibit significant spread in simulated snow water equivalent during the spring period [*Slater et al.*, 2001; *Frei et al.*, 2005; *Räisänen*, 2008]. Since the

[1]Climate Research Division, Atmospheric Science and Technology Directorate, Environment Canada, Toronto, Ontario, Canada.
[2]Alaska Division of Geological and Geophysical Surveys, Fairbanks, Alaska, USA.
[3]Department of Earth and Atmospheric Sciences, University of Alberta, Edmonton, Alberta, Canada.
[4]Climate Research Division, Ouranos, Environment Canada, Montreal, Quebec, Canada.
[5]Cryospheric Sciences Branch, NASA Goddard Space Flight Center, Greenbelt, Maryland, USA.

Published in 2011 by the American Geophysical Union.

Table 1. Melt Detection Algorithms and Data for Each Element of the Cryosphere Included in This Study

Cryosphere Element	Melt Detection Algorithm	Data Set, Resolution, and Reference	Name of Algorithm
Terrestrial snow	Multiple melt events; $\sigma^0 < 1.7$ dB of the previous 5 day average for three or more consecutive days; main melt event has the longest melt duration	QSCAT, 4.45 km [*Wang et al.*, 2008]	qs_terrestrial
Ice cap/sheet	$\sigma^0 < 3.0$ dB of winter mean for 3 or more consecutive days, or $\sigma^0 < 3.5$ dB of winter mean for 1 day	QSCAT, 2.225 km [*Sharp and Wang*, 2009]	–
Lake ice	$\sigma^0 < 4$ dB of winter mean for 2 or more consecutive days	QSCAT, 4.45 km [*Howell et al.*, 2009b]	–
CAA sea ice	absolute change in $\sigma^0 > 2$ dB of winter mean; a kriging interpolation method is applied to estimate spatially continuous onset dates	QSCAT, 4.45 km [*Howell et al.*, 2006]	qs_caa
Arctic sea ice	Multiple indicators: daily change in 37V, spectral gradient ratio for 37V and 19, P = Tb(19V) + 0.8Tb(37V)	SMM/I, 25 km [*Markus et al.*, 2009]	ssmi_early ssmi_melt

Arctic climate is particularly sensitive to spatial and temporal variations in snow and ice cover, climate models must simulate snow cover (and especially spring snowmelt timing) accurately in order to capture the variations and feedbacks in high-latitude climate. Validation of climate model simulations of snow cover and snowmelt processes is a challenge in the Arctic, where the surface observing network is sparse and persistent cloud cover and polar darkness hamper snow mapping from optical satellite sensors. These limitations translate into higher uncertainties in the available observational data sets compared to middle latitudes [*Brown and Frei*, 2007; *Brown and Mote*, 2009; *Roesch*, 2006].

[4] Summer sea ice extent has decreased dramatically over the past decade [*Stroeve et al.*, 2007] because of the advection of warm air masses by winds associated with a meridional atmospheric circulation pattern, coupled with a thinning ice pack [*Lindsay et al.*, 2009; *Overland et al.*, 2008; *Serreze et al.*, 2007; *Wang et al.*, 2009]. Previous studies indicate that the total amount of solar energy absorbed by sea ice during the summer melt season is strongly related to the timing of melt onset but only weakly related to the total duration of the melt season or the timing of onset of freezeup [*Perovich et al.*, 2007a, 2007b]. The timing of melt onset is significant because the solar incidence angle is greatest in the late spring, and changes in the surface albedo and the surface energy balance at this time propagate through the entire melt season, affecting the absorbed solar flux until the solar incidence angle is low again. *Stroeve et al.* [2006] found close correlation between regional melt onset timing and the amount of pan-Arctic sea ice in September, and *Howell et al.* [2009a] reported similar results from within the Canadian Arctic Archipelago (CAA).

[5] Satellite passive microwave data from the Scanning Multichannel Microwave Radiometer (SMMR, 1979–1987) and the Special Sensor Microwave/Imager (SSM/I, 1987 to present) and active microwave data from the SeaWinds scatterometer aboard QuikScat (QS, 1999–2009) have been widely used to detect snowmelt onset on various elements of the cryosphere because of their high sensitivity to the presence of liquid water in snow and their day/night, all-weather capability [e.g., *Abdalati and Steffen*, 1995; *Drobot and Anderson*, 2001a; *Howell et al.*, 2006, 2009b; *Markus et al.*, 2009; *Mote and Anderson*, 1995; *Rawlins et al.*, 2005; *Sharp and Wang*, 2009; *Smith*, 1998; *Takala et al.*, 2009; *Wang et al.*, 2005, 2008]. While those studies focused on separate components of the cryosphere, the aim of the present study is to provide an integrated melt onset data set for all elements of the Arctic cryosphere (north of 60°N) by combining active- and passive-microwave-derived melt onset estimates for the 2000–2009 period. This approach provides a unique data set for validating model simulations during the spring transition period when snow cover exerts the strongest feedback on the climate system [*Déry and Brown*, 2007; *Groisman et al.*, 1994; *Flanner et al.*, 2011]. Using this data set, we document the spatial and temporal variability in melt onset across the Arctic and evaluate the ability of a typical global climate model (GCM) used in the Fourth Intergovernmental Panel on Climate Change Assessment to capture the spring snowmelt onset timing during the most recent decade. Working with the new data set, we investigate the effects of vegetation and elevation on melt onset patterns, present the mean horizontal melt progression rate across the Arctic, and explore the role of melt onset timing in influencing sea ice extent.

2. Data and Methods

2.1. Snowmelt Detection Algorithms for Satellite Data

[6] Time series of both active and passive microwave measurements have been widely used for melt detection in the Arctic. During the transition from dry to wet snow, the radar backscattering coefficient (σ^0) decreases dramatically as surface scattering begins to dominate over volume scattering [*Ulaby et al.*, 1982]. The exception is over first-year sea ice, where increased σ^0 is observed with melt onset because of an accompanying increase in brine volume, which increases the dielectric permittivity and contributes to enhanced volume scattering [*Barber and Nghiem*, 1999]. For passive microwave observations, the microwave emissivity (ε) increases distinctly from dry to wet snow because of the much higher dielectric constant of water, resulting in an increase in the brightness temperature in accordance with the Rayleigh-Jeans approximation [*Ulaby et al.*, 1982, 1986]. These responses to melt onset provide the basis for melt detection using active and passive microwave data.

[7] Temporal variations in backscatter or brightness temperature allow identification of the date of melt onset. Threshold techniques have been applied to QS data to retrieve melt onset dates for terrestrial snow cover, lake ice, ice caps across the Arctic, and sea ice in the CAA. Multiple indicators have been used to determine the timing of Arctic sea ice melt onset from passive microwave data. Melt detection algorithms used for each surface type in this study are described briefly below and summarized in Table 1.

[8] 1. Terrestrial snow: Melt onset was detected if the daily QS σ^0 was 1.7 dB lower than the previous 5 day average for

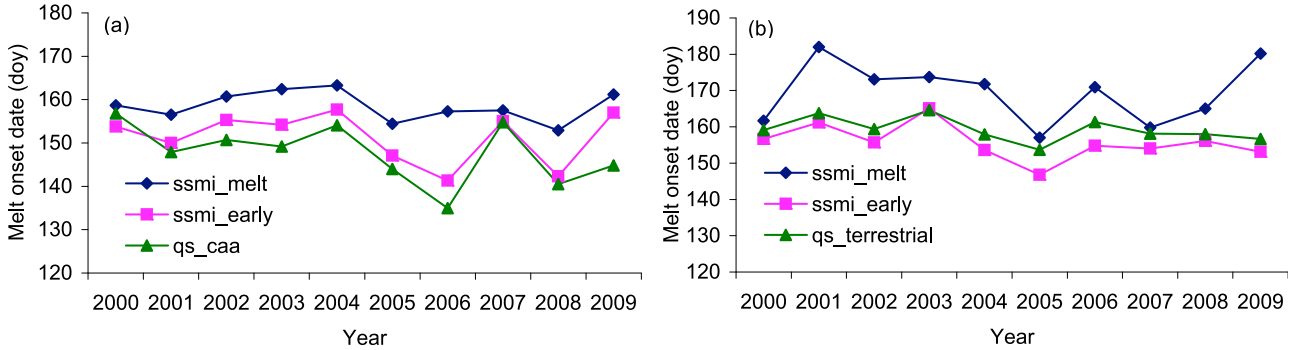

Figure 1. Annual MOD (day of year) from SSM/I and QS for sea ice regions in the (a) CAA and (b) central Arctic. See location of central Arctic region in Figure 3a.

three or more consecutive days. This algorithm, described by *Wang et al.* [2008], is capable of distinguishing "preliminary" melt events from the "main" melt event and identifies and excludes areas for which a snowmelt event cannot be identified (typically because of dense forest cover or very shallow snow) to prevent erroneous melt retrievals. The main melt onset date was used in this study; this date identifies when snow is wet but still fully covering the ground.

[9] 2. Ice caps/Greenland: On the basis of previous melt detection efforts [*Sharp and Wang*, 2009], an optimized single set of thresholds was developed to estimate melt onset for all the ice caps in the Arctic from QS data, including the Greenland Ice Sheet (GrIS). Onset was determined when σ^0 was either (1) 3.0 dB lower than the winter mean σ^0 for 3 or more consecutive days or (2) 3.5 dB lower than the winter mean for 1 day.

[10] 3. Lake ice: Melt onset over Great Bear Lake and Great Slave Lake was detected when QS σ^0 was 4 dB lower than the winter mean for 2 or more consecutive days [*Howell et al.*, 2009b]. We include only these two lakes as they are the only large lakes north of 60°N.

[11] 4. Canadian Arctic Archipelago (CAA) sea ice: Melt onset was estimated from QS data using a threshold of absolute change in σ^0 (increase for first year ice, decrease for multiyear ice) of more than 2 dB from winter conditions. The algorithm was applied to pixels identified as homogeneous first-year ice ($\sigma^0 < -18$ dB) or multiyear ice ($\sigma^0 < -11$ dB) during the winter season. A kriging interpolation method (following *Howell et al.* [2006]) was used to estimate spatially continuous patterns of onset dates in the CAA.

[12] 5. Sea ice outside the CAA: Melt onset on sea ice outside the CAA was estimated using SSM/I passive microwave data [*Markus et al.*, 2009]. The strength of the melt signal was determined by summing the normalized magnitudes of multiple melt indicators. The day with the greatest sum was taken as the "melt" onset day (hereafter referred to as "ssmi_melt"), and the second largest peak was taken as the "early melt" day (hereafter referred to as "ssmi_early"). "Early melt" is related to the transition period when transformation of the snowpack due to melt-freeze cycles begins. "Melt" is defined as the day after which free water is continuously present in the snowpack. "Early melt" was found to be closely related to melt onset from QS data [*Markus et al.*, 2009] and was therefore used in this study.

[13] All the algorithms described above have been validated using in situ observations and assessed against other available melt onset data sets within the studies listed in Table 1. We consider these algorithms to be the optimal methods for melt detection for each element of the cryosphere. An attempt was made to develop a melt detection threshold algorithm for the entire cryosphere using only QS data. For sea ice outside the CAA, QS-derived melt onset dates (not shown) were in close agreement with those from the passive microwave data for areas with landfast ice and multiyear pack ice. However, for some areas between the central pack ice and the coastal landfast ice, patterns of QS-derived melt onset dates were noisy: melt onset dates were often either abnormally early or abnormally late compared to those in neighboring grids. The Ku-band QS data are very sensitive to changes in the surface properties of sea ice resulting from lead development, ice motion, and ridging. Cases where extremely early melt onset was thought to be related to lead opening were confirmed by means of Moderate Resolution Imaging Spectroradiometer (MODIS) clear-sky composite images [*Luo et al.*, 2008]. Although similar issues were also seen in the results derived from passive microwave data, it was much less significant in terms of the area and frequency of grids affected. We therefore chose to use the passive microwave data for melt detection on sea ice outside the CAA.

[14] Considering the differences in the physical basis for melt detection using active and passive microwave data, an important question is whether the melt onset results derived from passive (e.g., SSM/I) and active (e.g., QS) microwave data are consistent. *Markus et al.* [2009] showed that the 2000–2007 mean "early melt" onset dates from passive microwave data agreed well with melt onset dates derived from QS data on sea ice in the CAA. We also found that the melt onset dates (MODs) over sea ice in the CAA derived from passive microwave [*Markus et al.*, 2009] and QS data [*Howell et al.*, 2006] were consistent in the 2000–2009 period (Figure 1a). The mean difference between the two data sets for the period was 3.6 days, with a standard deviation of 4.0 days. To test this correspondence further, we applied the QS melt detection algorithm developed in *Wang et al.* [2008] for the terrestrial Arctic to central Arctic sea ice and compared estimates derived from QS and passive microwave data for a region of the central Arctic (see location in Figure 3a). The annual melt onset dates derived from the two data sets are closely covariant, with a mean difference of 3.6 days and a standard deviation of 2.2 days (Figure 1b). This agreement justifies our

use of the combined active and passive microwave data set to generate an integrated melt onset data set for the entire Arctic cryosphere.

[15] Using the algorithms shown in Table 1, MODs were determined for each component of the cryosphere and combined into a single data set for each year of the 2000–2009 period. This study uses two data sources: (1) enhanced-resolution products produced from QS L1B data with the scatterometer image reconstruction algorithm [*Early and Long*, 2001], available from the Brigham Young University Centre for Remote Sensing [*Long and Hicks*, 2005]; and (2) daily averaged brightness temperatures from SSM/I [*Maslanik and Stroeve*, 1990], available from the National Snow and Ice Data Center in Boulder, Colorado. For visualization purposes, we downscaled the 25 km passive-microwave-derived sea ice data set and scaled up the 2.225 km QS-derived data set for ice caps to the 4.45 km QS polar stereographic grid using a nearest neighbor method. The mean melt onset dates (MMOD), along with the standard deviation, were computed for the most recent decade. The standard deviation was computed only for areas where melt occurred in at least 5 years in the 10 year period. All statistics were calculated from the original-resolution data to avoid artifacts due to data resampling.

[16] Our study area lies north of 60°N and is assumed to be completely snow covered prior to the spring melt period. The active- and passive-microwave-derived MOD is primarily associated with the early stage of spring snowmelt. However, snowmelt onset is sometimes not detected in tundra regions with shallow snow cover or in regions with dense forest cover [*Wang et al.*, 2008]. For areas of relatively thin ice cover, such as the marginal sea ice zone, the melt signal is not always clear. In these areas, MOD was defined following *Markus et al.* [2009] as the day on which ice concentration dropped below 80% for the last time before becoming ice-free. Hereafter in this paper we use "MMOD" to refer to the 10 year mean melt onset date during the period 2000–2009; we use "MOD" to refer to melt onset date in all other situations, such as the MOD at a specific year for a specific component of the cryosphere.

2.2. Simulated Snowmelt Onset in CGCM3

[17] The pan-Arctic melt onset data set described above was used to evaluate the simulated melt onset in the third version of the Canadian Coupled Global Climate Model (CGCM3) [*Flato and Boer*, 2001; *Scinocca et al.*, 2008], which used a T63 horizontal resolution (approximately 330 km or 2.81° × 2.81°) and 31 vertical atmospheric layers. The particular CGCM3 simulation used in this study was integrated from 1850 to 2000 using historical forcings and then continued using forcings from the Special Report on Emission Scenarios A1B scenario [*Nakicenovic et al.*, 2000] beyond year 2000. We then compared CGCM3 mean Arctic snow cover extent over the April-June melt period with that yielded by other Coupled Model Inter-comparison Project (CMIP3) GCMs [see *Brown and Mote*, 2009, Table 2] and the NOAA satellite data set (not shown); the comparison reveals that the seasonal ablation timing and rates in CGCM3 are similar to that from the satellite data and the GCM ensemble average. The annual melt onset date at each grid point north of 60°N was determined from daily values of snowmelt runoff simulated by CGCM3 [*Flato and Boer*, 2001; *Scinocca et al.*, 2008]; these values were provided by the Canadian Centre for Climate Modeling and Analysis (CCCma), as this variable is not available from the CMIP3 archive. Melt onset was assumed when snowmelt runoff was greater than zero for 3 or more consecutive days. Mean values of melt onset date and standard deviation were computed over the 2000–2009 period to match the satellite record.

[18] In CGCM3, snow cover and snowmelt processes are treated in the Canadian Land-surface Scheme (CLASS V2.7) over land areas [*Verseghy*, 1991; *Verseghy et al.*, 1993] and in a thermodynamic model over sea ice, as outlined by *Flato and Brown* [1996]. CLASS has three soil layers, a snow layer, and a vegetation canopy with physically based calculations of heat and moisture transfers at the surface and across layer boundaries. Snow is treated as a variable depth fourth "soil" layer and snow-covered and snow-free areas are treated separately [*Brown et al.*, 2006]. On ice caps and GrIS, glacier ice at the bottom of the snowpack is treated as "soil" layers without pores. The energy balance of the snowpack is solved iteratively for surface temperature, taking into account incoming shortwave and longwave radiation, snow albedo and density, sensible and latent heat exchanges, and the ground heat flux. If the simulated surface temperature is above freezing, the surface temperature is reset to 0°C, and the excess energy is applied to melting snow. The amount of liquid water percolation through the snowpack (snowmelt or liquid precipitation) is determined from the heat balance of the snowpack. If the snowpack temperature is below freezing, liquid water refreezes and the heat released warms the snowpack. Once the snowpack is isothermal, all meltwater is assumed to percolate through the snowpack and contribute to snowmelt runoff.

[19] To assess simulated snowmelt onset patterns from CGCM3 (hereafter referred to as "model" or "simulated" MMOD), the combined active- and passive-microwave-derived data set (see section 2.1, hereafter referred to as "satellite" or "observed" MMOD) was regridded to the model grid (~2.81° × 2.81° latitude-longitude grid) by averaging all the grid cells whose centers fall within the model grid cell. In the following sections, we present the satellite results on the model grid side by side with the model results. We compare the spatial and temporal distribution patterns of the simulated and the observed MMOD and attempt to explain the observed differences between them. We investigate whether or not the observed differences exhibit any latitudinal or longitudinal dependencies and, if they do, whether they are related to vegetation or topography, or both, in the terrestrial Arctic.

2.3. Analysis Methods and Other Data Sets

[20] Forest cover and topography can exert large effects on MMOD across the terrestrial Arctic [*Wang et al.*, 2008]. Quantitative information about forest cover and topography is therefore helpful in interpreting the spatial distribution of MMOD. Tree fraction estimates (percentage of forest in each grid) for each QS grid were aggregated from the 500 m resolution MODIS vegetation continuous field product [*Hansen et al.*, 2006]. Surface elevations were obtained from the Global 30 Arc-second Elevation Data set (GTOPO30), developed by the U.S. Geological Survey (http://www.webgis.wr.usgs.gov/globalgis/gtopo30/gtopo30.htm), which uses the same grid as the QS data. Multiple regression of

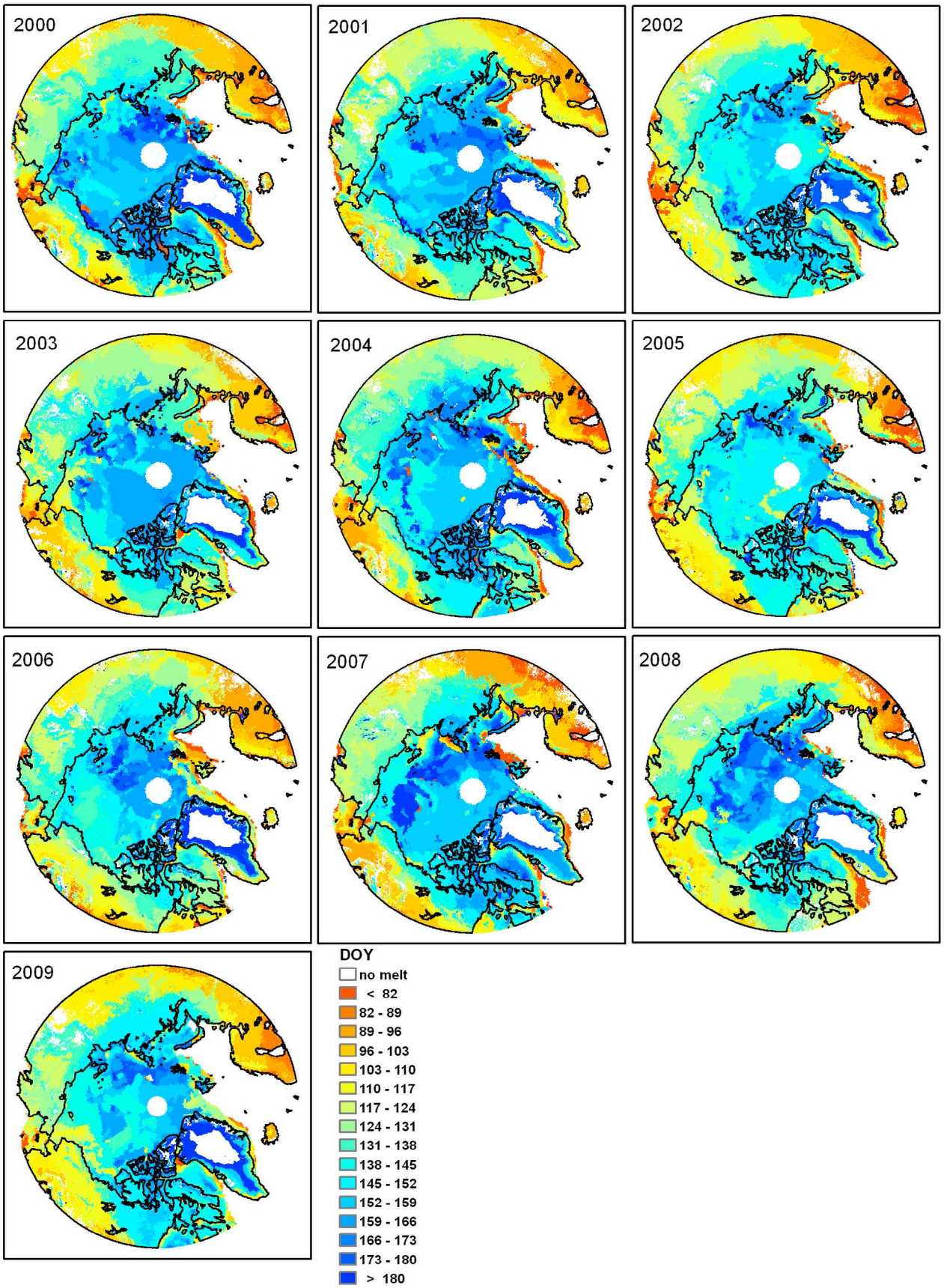

Figure 2. Map of integrated pan-Arctic melt onset date (day of year) in each year during 2000–2009.

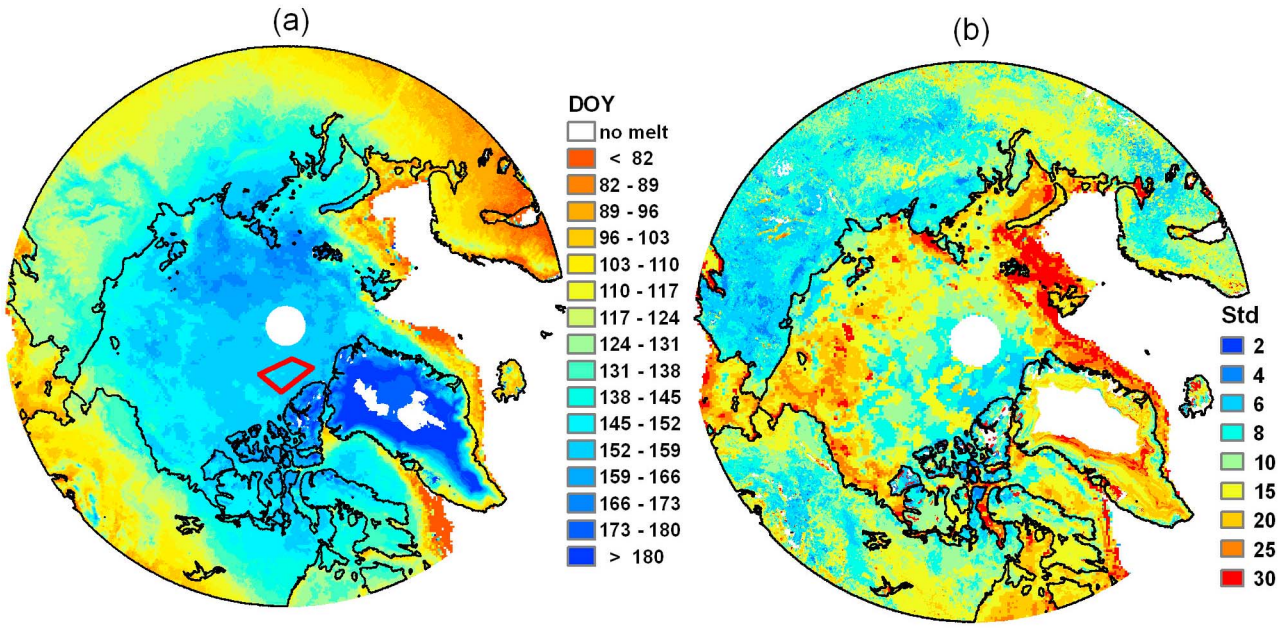

Figure 3. (a) Mean melt onset date (day of year) and (b) the standard deviation (days) during 2000–2009. The red polygon in the central Arctic in Figure 3a represents the region shown in Figure 1b.

MMOD against tree fraction, elevation, and latitude was conducted to investigate the combined effects of these geographic variables on melt onset in the North American and Eurasian Arctic mainland. Simple linear regression between MMOD and each individual variable was also performed to provide an indication of the relative importance of the different variables as influences on MMOD.

[21] We also investigated the effects of elevation on MMOD at the regional scale. The mean vertical melt progression rate, dz/dMMOD (**N**, m d^{-1}) was obtained through linear regression analysis between elevation and MMOD over a 21 × 21 moving window. The size of the moving window (~100 km) is about the same as that used by *Brown et al.* [2007] to document the elevation dependence of spring snow cover duration (SCD) analysis. Only statistically significant regression results are reported.

[22] The mean horizontal melt progression rate (**M**, km d^{-1}) was computed from the average absolute gradient in MMOD between each grid point and the eight adjacent points on the satellite grid or the four adjacent points on the model grid. This variable provides information on melt dynamics and identifies regions with strong feedback potential. To remove noise, a 5 × 5 spatial averaging was applied to MMOD on the satellite grid before the calculation. A cutoff was applied for **M** > 330 km d^{-1} as it approaches infinity as the spatial gradient in MMOD approaches zero.

[23] To examine whether or not there are latitudinal or longitudinal dependencies in the simulated and observed MMOD and their difference, zonal and meridional averages of MMOD were computed on the model grid for every grid in the latitude direction (~2.81°) and for every three grids in the longitude direction (~8.44°).

[24] Monthly sea ice extent data were obtained from the National Snow and Ice Data Center sea ice index [*Fetterer et al.*, 2009], which is derived from passive microwave data using the NASA Team algorithm [*Cavalieri et al.*, 1996]. The relationship between melt onset timing and monthly sea ice extent north of 60°N was investigated through correlation analysis. This analysis was performed between sea ice extent and MMOD over the terrestrial Arctic mainland (excluding Arctic islands and Greenland) and on the Arctic sea ice (excluding the Bering Sea). The linear trend in each data set was removed prior to the analysis.

[25] Monthly air temperature (April to June) at 850 hPa pressure level was obtained from the National Centers for Environmental Prediction/National Center for Atmospheric Research Reanalysis 1 data set [*Kalnay et al.*, 1996]. The 850 hPa level was chosen because it is generally above the main topographic features across the continental Arctic. The significance levels of the regressions and correlations were determined using a two-tailed Student's *t* test. All reported correlations are statistically significant at a significance level of 0.05.

3. Results and Discussion

3.1. Spatial and Temporal Variability in Melt Onset From Satellite Observations

[26] There are large annual and interannual variations in MOD within and between each component of the cryosphere (Figures 2 and 3). On average, melt starts in the middle to end of March (day of year (DOY) 75~90) in the boreal forest and the marginal seas, with the date of melt onset becoming progressively later with increasing latitude. In the Arctic tundra, melt does not typically start until late May or early June (~DOY 150). On the Arctic sea ice, melt advances rapidly during May and reaches the central Arctic by mid-June (~DOY 165). In the terrestrial Arctic, the spatial distribution of MOD is closely related to land cover,

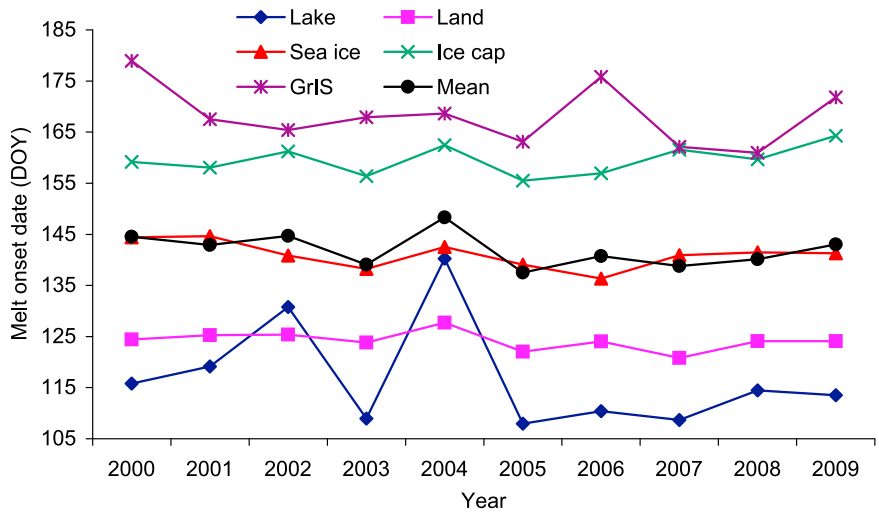

Figure 4. Annual MOD (day of year) for each component of the cryosphere during the period 2000–2009.

latitude, and topography, while on the Arctic sea ice it is very patchy, and there is no obvious latitudinal dependency in the annual MOD maps (Figure 2). In the central Arctic, the mean melt onset pattern is spatially asymmetric, with the latest melt onset in the northern Laptev and Kara Seas (Figure 3a). Melt occurs much later on the ice caps and GrIS than on land and sea ice because of the lower air temperatures associated with their high elevations. Melt occurs everywhere on the surface of most of the Arctic ice caps every summer except in some high-elevation areas in the Queen Elizabeth Islands (QEI) and GrIS [*Sharp and Wang*, 2009; *Wolken et al.*, 2009]. There are large interannual variations in melt extent on the GrIS (Figure 2). During the period 2000–2009, melt did not reach the summits of the Agassiz Ice Cap in 2002 and Northern Ellesmere Island Ice Fields in 2002 and 2004. In contrast, the annual melt extent on the GrIS reached a maximum in 2002. These results suggest that the annual timing and extent of surface melt on the ice caps and GrIS is influenced by regional atmospheric conditions [*Wang et al.*, 2005, 2007].

[27] On average, 2005 had the earliest and 2004 had the latest MOD over the entire Arctic (Figure 4 and Table 2). Large lakes exhibit relatively larger interannual variations in MOD than the other components of the cryosphere (Table 2). These variations arise because the two large lakes in northern Canada cover only a small area, while the other components either extend across the pan-Arctic or cover a large area. The earliest/latest MOD occurred in different years for different components of the cryosphere (Table 2). For example, it was 2007/2004 on the Arctic mainland, but 2006/2001 over the Arctic sea ice. Although 2007 marked the largest loss in summer sea ice during the most recent decade, melt onset timing on the Arctic sea ice was not particularly early in 2007. The earliest/latest MOD occurred in 2005/2009 on the ice caps and in 2008/2000 on the GrIS.

[28] Across the Arctic, the interannual variability in melt onset timing is generally larger on sea ice than on land, especially in the marginal seas (Figure 3b). This variability occurs because melt onset is influenced by ocean currents, sea ice motion, and mixed pixel effects in the marginal ice zone (e.g., melt onset can be associated with decreases in ice concentration rather than with regional thermodynamic processes [*Markus et al.*, 2009]). In addition, spring weather is probably more variable near areas of ice-free ocean than in the land- or ice-locked areas, as suggested by *Anderson and Drobot* [2001]. Increased synoptic activity in the Arctic spring accounts for why the interannual variability is larger overall on sea ice [*Belchansky et al.*, 2004; *Serreze et al.*, 1995] than on land, where the variability is to some extent suppressed by land cover and topography. Melt onset also exhibits large interannual variability at high elevations of the GrIS (Figure 3b). This occurs because distinct melt events cause melt onset at different elevations of the ice sheet [*Wang et al.*, 2007]. Only the most intense melt events extend to the higher elevations of the ice sheet, and the timing of these events is highly variable.

3.2. Relationship Between MMOD and Latitude and Tree Fraction

[29] The spatial distribution of MMOD is closely related to land cover, latitude, and topography in the terrestrial Arctic (Figure 3a). Multiple regression of MMOD against tree fraction, latitude, and elevation indicates that tree

Table 2. Annual MOD for Lakes, Continental Land, Sea Ice, Ice Caps, and GrIS[a]

Year	Lake	Land	Sea Ice	Ice Cap	GrIS	Mean
2000	115.8	124.4	144.4	159.1	**178.9**	144.5
2001	119.1	125.3	**144.7**	158.1	167.5	142.9
2002	130.8	125.4	140.9	161.2	165.4	144.7
2003	108.9	123.8	138.2	156.4	167.9	139.1
2004	**140.2**	**127.7**	142.5	162.4	168.6	**148.3**
2005	**107.9**	122.0	139.1	**155.5**	163.1	**137.5**
2006	110.4	124.1	**136.3**	156.9	175.8	140.7
2007	108.6	**120.8**	140.9	161.6	162.1	138.8
2008	114.4	124.1	141.5	159.6	**161.0**	140.1
2009	113.5	124.1	141.3	**164.3**	171.8	143.0
Mean	117.0	124.2	141.0	159.5	168.2	142.0
Std. Dev.	10.6	1.9	2.6	2.9	5.9	3.3

[a]Bold values represent earliest or latest melt onset date in each component.

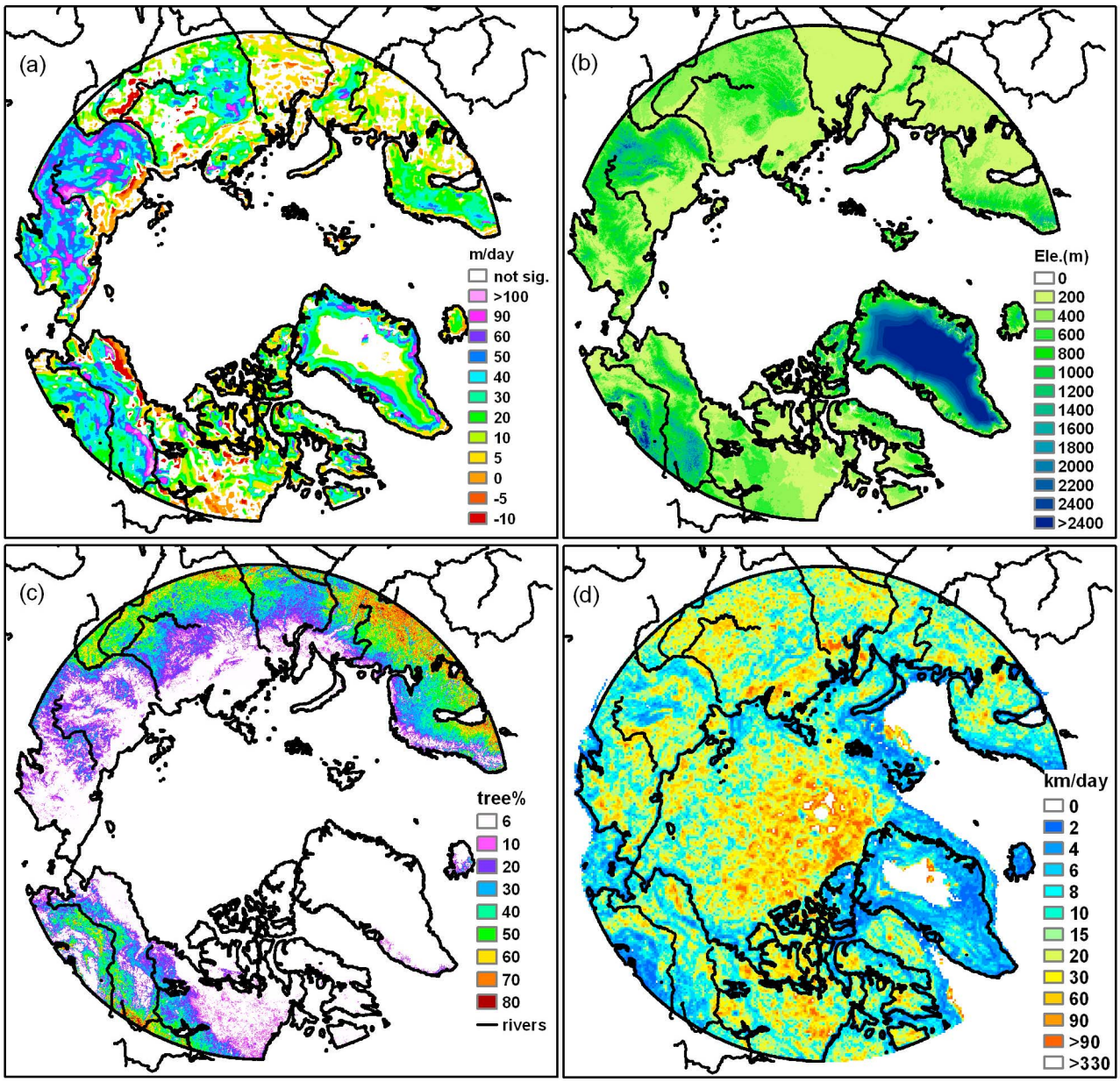

Figure 5. The relationship between MMOD and (a) elevation (m d^{-1}), (b) elevation (m), (c) tree fraction (%), and (d) the mean horizontal melt progression rate (km d^{-1}).

fraction and latitude are statistically significant influences explaining 61% and 66% of the variance in MMOD in the North American and Eurasian Arctic mainland, respectively. As elevated terrain occupies only a small fraction of the total land area, elevation does not exert a significant influence on MMOD at the continental scale. Simple linear regression results show that tree fraction exerts a stronger influence on MMOD (r = 0.72) than latitude (r = 0.60) in the North American Arctic, while these variables appear to exert equal influence in the Eurasian Arctic ($r \approx 0.74$). However, tree fraction and latitude are significantly correlated with each other in Eurasia (r = 0.65), but not in North America. This result suggests that tree fraction has a stronger influence on MMOD than latitude in the terrestrial Arctic.

3.3. Relationship Between MMOD and Elevation

[30] Most of the Arctic (58% of the total land area) exhibits a significant positive relationship between MMOD and elevation that is consistent with a decrease in air temperature with elevation (Figure 5a). Relatively high progression rates (**N** > 50 m d^{-1}) are mainly located in high-relief areas (Figure 5b), such as the mountainous areas of western North America, eastern Siberia, Scandinavia, and ice caps in the QEI and Greenland. The highest rates are generally concentrated in the foothills of the mountains and at low elevations on the ice caps and GrIS. Low progression rates (**N** < 20 m d^{-1}) are mainly located in areas with limited surface relief, such as the flat areas along the Ob river basin, boreal forest areas in northern Europe, and in the Canadian

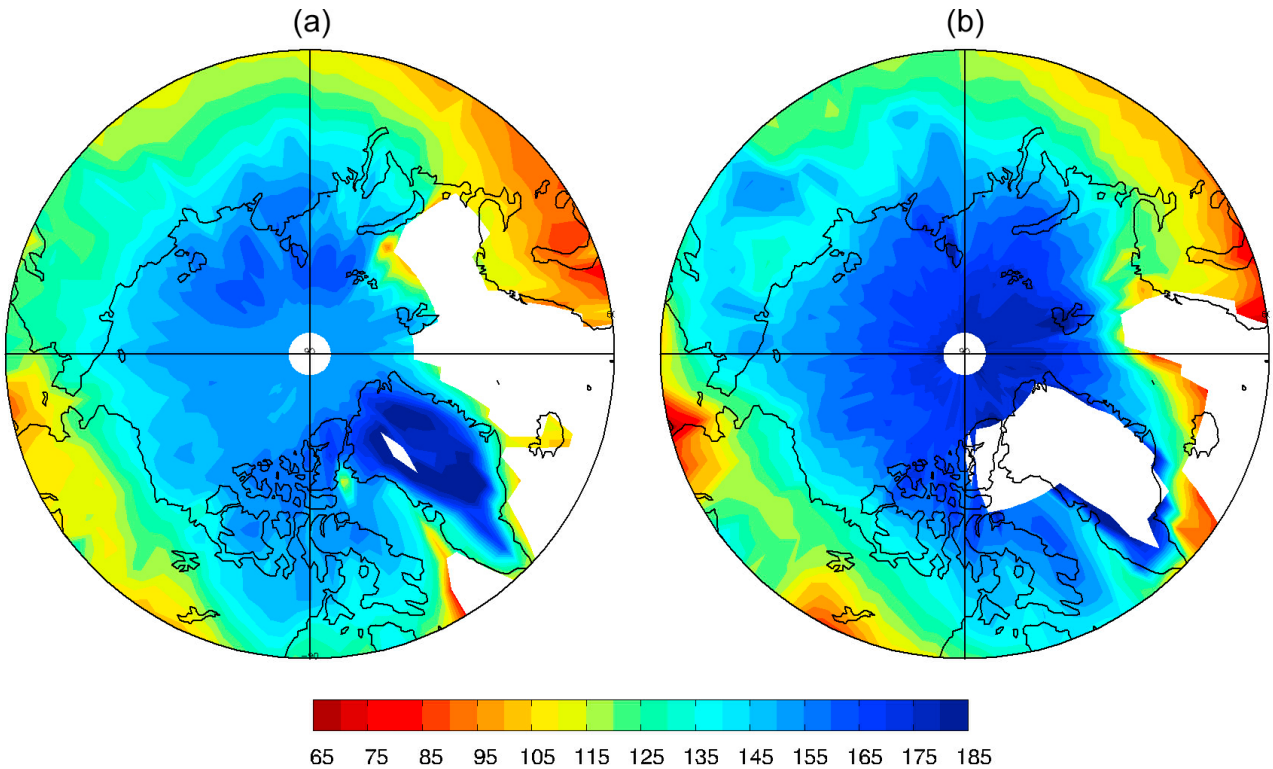

Figure 6. The mean melt onset date (day of year) during 2000–2009 from (a) satellite and (b) CGCM3.

Arctic tundra. Most of the areas without a statistically significant relationship between MMOD and elevation are found in these areas of flat terrain. Almost the entire observed range in **N** can be found on the GrIS, from the highest rate at low elevations to an intermediate rate at mid-elevations to the lowest rate at the highest elevations reached by melt. The grid points with a significant positive relationship between MMOD and elevation have a mean melt onset progression rate of 24.5 m d^{-1} across the terrestrial Arctic (excluding Greenland).

[31] Some small regions (6% of total land area) exhibit a significant negative relationship between MMOD and elevation (Figure 5a). These tend to be located in areas with little vertical variation in surface elevation in the interiors of the continents and also on the North Slope of Alaska. The grid points with significant negative relationships have a mean value of **N** = −11.1 m d^{-1} and a mean elevation of 194 m. *Brown et al.* [2007] also found negative relationships between spring snow cover duration (SCD) and elevation in northern Canada (see their Figure 7). They attributed this result to wind scour of snow on exposed uplands with less vegetation. This explanation is supported by *Déry et al.* [2004], who showed that snow cover on the North Slope of Alaska was preferentially redistributed from windward slopes and hilltops onto lee slopes and lowland areas because of interactions between the prevailing winds, vegetation, and topography. We computed dz/dSCD for the spring period over the pan-Arctic region following *Brown et al.* [2007] (not shown), and the areas with significant negative relationship to elevation agreed closely with the areas of negative dz/dMMOD shown in Figure 5a.

3.4. Comparison of Observed and Simulated Melt Onset

[32] Melt onset derived from satellite microwave sensors is associated with the occurrence of surface melting of the snowpack, which is different from the melt runoff derived from CLASS/CGCM3, which requires the warming of the snowpack to 0°C. However, the timing of melt onset on land from QS data corresponds to the main melt period [*Wang et al.*, 2008] and should therefore be compatible with the definition used in CLASS. This assumption is strongly supported by the good agreement between the CGCM3 and satellite-derived MMOD across most of the terrestrial Arctic (Figure 6, Table 3). Late MMOD from CGCM3 in eastern Siberia corresponds to a region where the simulated surface temperature showed the largest variability among all the CMIP3 models [see *Randall et al.*, 2007, Figure S8.2]; the late melt onset is probably related to a combination of positive snow water equivalent bias and cold temperature bias (thus delayed snowmelt onset) in CGCM3 and other models [*Brown and Mote*, 2009; *Randall et al.*, 2007].

[33] There is an apparent delay between the simulated and observed MMOD over most sea ice areas (Figure 6). This delay is probably due to (1) a cold temperature bias and thus delayed melt onset over sea ice in CGCM3 [*Chapman and Walsh*, 2007; *Karlsson and Svensson*, 2011] or (2) "early melt" on sea ice associated with the melt-freeze transition period [*Markus et al.*, 2009], which may indeed be earlier than the simulated melt runoff onset timing in CGCM3, or (3) a combination of both effects. Since by definition "melt" (see section 2.1) should correspond to the development of an isothermal snowpack [*Markus et al.*, 2009], we

Table 3. Zonal Averaged MMOD From CGCM3 and Satellite and Their Differences[a]

Latitude (°N)	CGCM3 (DOY)	Sat_early (DOY)	Diff1 (days)	Sat_melt (DOY)	Diff2 (days)
60	111.4	110.2	1.2	113.5	−2.1
63	122.3	116.2	6.2	117.5	4.9
66	130.6	124.6	6.0	125.9	4.7
68	136.8	134.2	2.7	136.6	0.3
71	141.8	145.3	−3.5	148.8	−7.0
74	151.5	152.3	−0.8	152.7	−1.2
77	159.9	149.1	10.8	155.4	4.5
80	167.0	156.7	10.3	163.5	3.6
82	170.7	156.1	14.6	160.0	10.7
85	172.4	152.4	20.0	160.9	11.4
88	175.9	150.9	25.0	159.1	16.7

[a]Column definitions: sat_early, algorithm "ssmi_early" on sea ice was used in the satellite data set; sat_melt, algorithm "ssmi_melt" on sea ice was used in the satellite data set; diff1, difference between CGCM3 and sat_early; diff2, difference between CGCM3 and sat_melt.

also examined the MMOD map produced from the "melt" onset data set on sea ice. Simulated MMOD shows better agreement with the "melt" data set than with the "early melt" data set (Figure 7a). However, simulated MMOD is still later than the satellite observations, especially in the central Arctic (Figure 7a and Table 4). For areas near the North Pole, the simulated MMOD is in late June, which is about 2 to 3 weeks later than in the satellite observations. Delayed melt onset on sea ice maintains a high simulated surface albedo for a prolonged period in early summer, which would reduce the absorption of solar radiation at the surface and reinforce the cold temperature bias in the model [*Chapman and Walsh*, 2007; *Karlsson and Svensson*, 2011]. The latest MMOD in the satellite data occurs in the Laptev and Kara Seas, while in the CGCM3 simulations it occurs in the east central Arctic. In addition, sea ice extent in the North Atlantic Ocean inferred from the MMOD maps is greater in CGCM3 than in the satellite data (Figure 6).

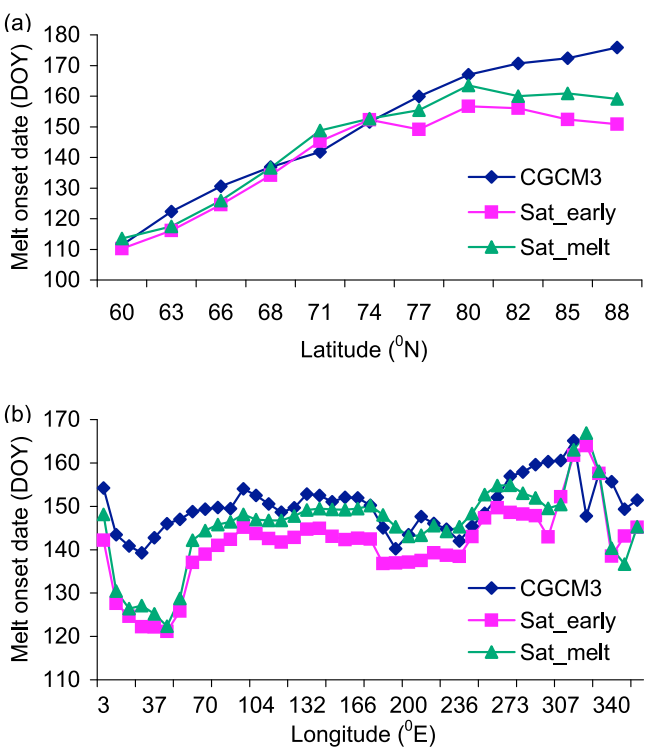

Figure 7. (a) Zonal and (b) meridional averaged MMOD from satellite observations and CGCM3 simulations. "Sat_early" represents MMOD using "ssmi_early" for sea ice, and "Sat_melt" represents MMOD using "ssmi_melt" for sea ice. Latitudinal zones above 74°N in Figure 7a mainly cover the Arctic Ocean; this is the region where the simulated and observed MMOD diverge.

[34] In contrast to satellite observations (Figure 6a), melt was not detected in the northern QEI and GrIS in CGCM3 (Figure 6b): the surface air temperature simulated by CGCM3 remained below freezing throughout the spring and summer in those areas. For example, the 2001–2005 mean July surface air temperature was only −3.6°C for the CGCM3 grid cell containing the weather station at Alert on the north coast of Ellesmere Island, while the observed mean July air temperature at Alert was 3.6°C for the same period. Although the simulated surface temperature did reach the freezing point occasionally, and surface melting probably occurred during some summers, melt did not reach the bottom of the snowpack (snowmelt runoff = 0.0) in any summer during the period 2000–2009. This result is consistent with the cold annual mean temperature bias in this region and over the Arctic sea ice for CGCM3 shown by *Chapman and Walsh* [2007] (their Figure 2). *Karlsson and Svensson* [2011] showed that in nine CMIP3 models the surface skin temperature over the Arctic sea ice tended to be the coldest in almost every month in CGCM3 (their Figure 3g).

[35] Grid cells for QEI and coastal GrIS are contaminated with sea ice because of the coarse model grid (~2.81° × 2.81°). Cold temperature biases in the northern QEI and GrIS grid cells are probably reinforced by the ice-albedo feedback mechanism associated with the cold temperature bias and delayed melt onset in the neighboring sea ice grids, as discussed just above.

[36] The largest meridional difference between the simulated and the observed MMOD occurs in areas from 0°~60°E and 290°E~360°E longitude (Figure 7b). This difference is due to the fact that the latest melt onset on sea ice in CGCM3

Table 4. Correlations Between Detrended Annual MOD and Monthly Sea Ice Extent[a]

Month	Land 00–09[b]	Sea Ice 00–09[b]	Land (lag 1 yr)[c]	Sea Ice (lag 1 yr)[c]	Sea Ice 90–99[d]
Jan	0.29	0.34	−0.14	0.38	−0.35
Feb	0.45	0.40	−0.34	0.38	−0.10
Mar	0.34	0.46	−0.07	0.58	−0.40
Apr	0.23	0.47	−0.05	**0.70**	−0.20
May	−0.11	0.56	0.07	**0.71**	0.00
Jun	0.05	0.49	−0.09	−0.06	**0.87**
Jul	**0.72**	0.17	−0.16	0.24	**0.84**
Aug	**0.63**	0.13	−0.22	0.37	**0.89**
Sep	0.56	−0.20	−0.03	0.33	**0.75**
Oct	0.49	−0.26	−0.19	0.48	0.55
Nov	0.44	**0.65**	−0.12	0.44	0.12
Dec	0.45	0.46	−0.18	0.06	0.26

[a]Bold values represent significant correlations ($p < 0.05$).
[b]Simultaneous years 2000–2009.
[c]Sea ice extent lagged one year (2001–2010).
[d]Years 1990–1999.

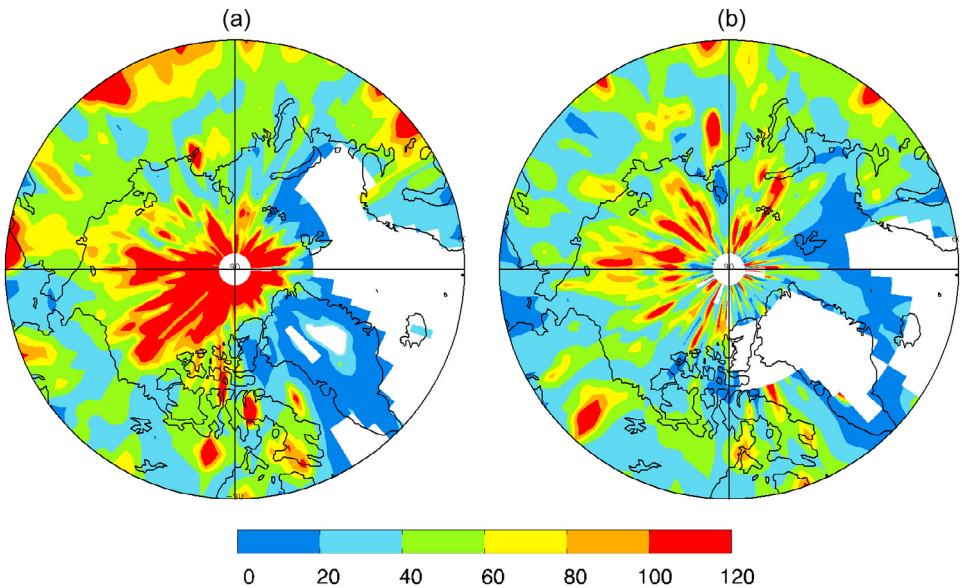

Figure 8. The mean horizontal melt progression rate (km d^{-1}) of MMOD from (a) satellite and (b) CGCM3.

occurs in those areas, that is, the Atlantic sector near the North Pole (Figure 6b). In addition, greater sea ice extent (as inferred from the MMOD maps in Figure 6) in the Barents Sea (0°~60°E longitude), Baffin Bay, south of Greenland, and the Greenland Seas (290°E~360°E longitude) in CGCM3 than in the satellite data (Figures 6a and 6b) also contributes to the large differences in areas from 0°~60°E and 290°E~360°E longitude.

3.5. Mean Horizontal Melt Progression Rate

[37] The mean horizontal progression rate (**M**, km d^{-1}) of MMOD in the terrestrial Arctic is closely related to land cover and topography (Figures 5b–5d). In general, melt onset advances rapidly (**M** > 30 km d^{-1}) where there are limited variations in land cover or elevation, as over most of the boreal forest and tundra regions. Slow progression (**M** < 10 km d^{-1}) of melt onset occurs mainly in high-relief areas and in the forest-tundra transition zones, such as areas along all the major mountain ranges (elevation >1200 m in Figure 5b), on the ice caps and GrIS, in the areas between the Great Slave and Great Bear Lakes, and in northern Russia. It also occurs within a narrow belt along the Arctic coast; this pattern is likely related to the small differences in melt onset date derived from QS data on land and from passive-microwave data on sea ice, as discussed in section 2.1. Over the Arctic sea ice, most of the western and central Arctic exhibits rapid melt progression (**M** > 60 km d^{-1}), which suggests that melt onset on sea ice is influenced by large-scale atmospheric circulation patterns [*Belchansky et al.*, 2004; *Drobot and Anderson*, 2001b]. Melt onset advances especially slowly in the northern Atlantic and northern Pacific (**M** < 8 km d^{-1}), as is especially evident in the maps produced on the model grid shown in Figure 8, such as in the Bering Sea, Baffin Bay, and Greenland and Barents Seas. This phenomenon is probably related to southward advection of sea ice counteracting the northward advance of melt onset [*Sorteberg and Kvingedal*, 2006; *Zhang et al.*, 2004, 2010]. For example, in the Bering and Barents Seas, melt starts as early as mid-March in the periphery (Figure 6a, DOY = 85), while melt does not occur until mid to late April in the interior (DOY = 120).

[38] While the spatial distribution pattern of the mean horizontal melt progression rate tends to be more uniform on the model grid than on the satellite grid (Figure 5d and Figure 8a), the main patterns of **M** are similar. The high progression rates in boreal forest regions that are evident from the satellite map are less pronounced in the CGCM3 map and present only in limited areas (such as in northern Europe, Russia, and southern Alaska). The CGCM3 map shows a high-**M** area in northwest Canada, while **M** is much lower for the same area in the satellite map. This pattern is reversed in the eastern Canadian Arctic, where several high-**M** regions in the satellite map are not evident in the CGCM3 map. These differences are probably related to the coarse

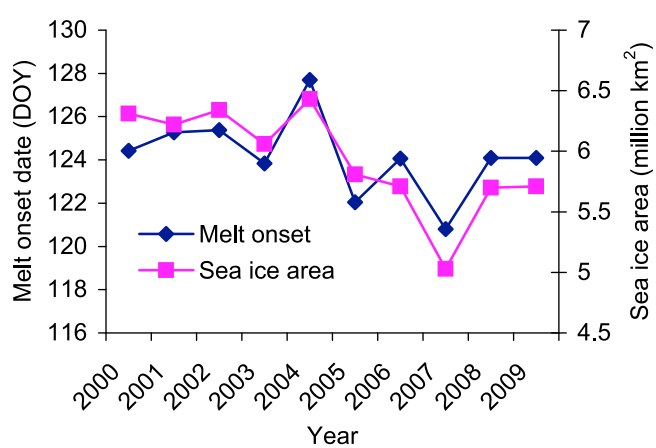

Figure 9. Annual MOD on land (day of year) and July sea ice area ($km^2 \times 10^6$).

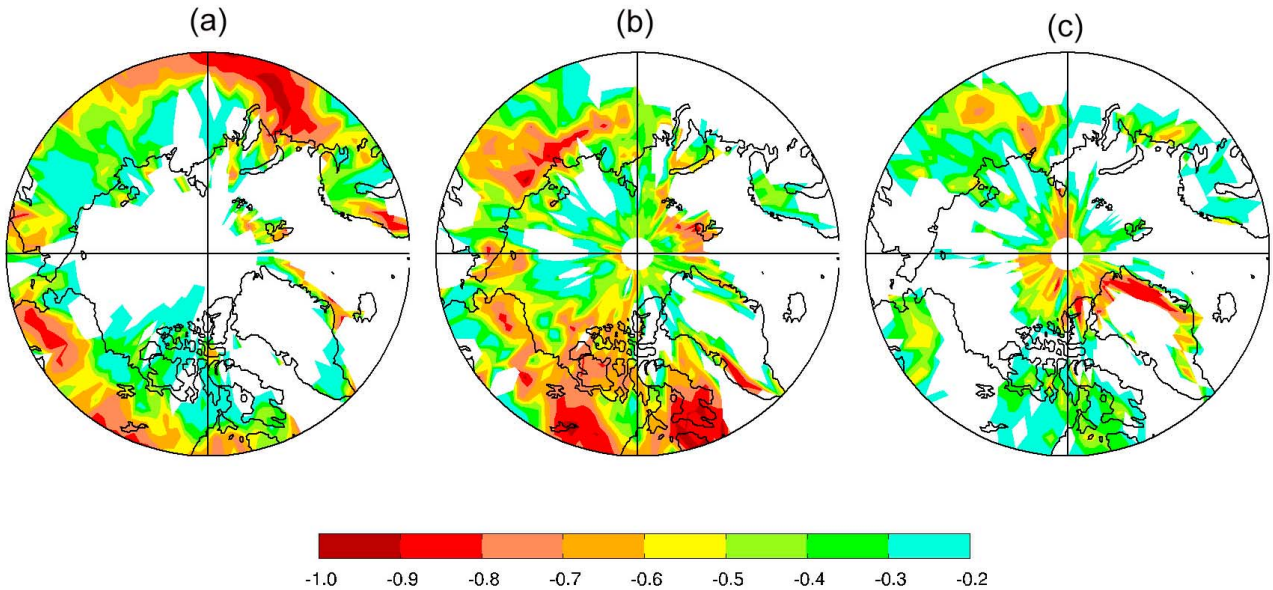

Figure 10. Correlations between annual MOD and air temperature: (a) April, (b) May, (c) June. Areas with $r < -0.6$ represent significant relationship at $p < 0.05$ level.

model grid that does not resolve the complex topography in the mountainous areas of northwest Canada, nor the complex land/sea boundaries of the eastern Canadian Arctic. The largest difference is found in the central Arctic, where **M** from satellite increases dramatically to more than 100 km d^{-1} in most areas, while **M** from CGCM3 exhibits high values over only limited areas. This behavior is consistent with the cold temperature bias in the model and delayed melt onset in the simulated MMOD over central Arctic sea ice, as discussed earlier.

3.6. Relationships Between Melt Onset and Sea Ice Extent

[39] For the period 2000–2009, MOD on sea ice is significantly correlated only with November sea ice extent (Table 4). This result may indicate that early melt onset (thus more heat absorbed in the ocean) contributes to delayed sea ice freezeup in the fall, which may in turn result in less sea ice extent in the following spring. This explanation is supported by the significant correlations between melt onset on sea ice and 1 year lagged sea ice extent in the spring (April and May, Table 4). The lack of significant correlations between MOD and summer sea ice extent during the most recent decade is probably due to thinner ice that is more vulnerable to other factors, such as anomalous warm winds, unusual atmospheric circulation patterns, and enhanced absorption of shortwave and longwave radiation, which have all been shown to have contributed to the rapid decline in summer sea ice extent [*Graversen et al.*, 2011; *Lindsay et al.*, 2009; *Nghiem et al.*, 2007; *Overland et al.*, 2008; *Perovich et al.*, 2008]. Melt onset timing on sea ice was significantly correlated with summer sea ice extent (June to September) during the decade 1990–1999 (Table 4), when sea ice thickness had not decreased as much as in the recent decade [*Lindsay et al.*, 2009; *Nghiem et al.*, 2007].

[40] In contrast, MOD on the Arctic mainland is significantly correlated with both July and August sea ice extent (Table 4). The annual mean melt onset date on land and July sea ice area are closely covariant (Figure 9). Melt onset on land typically occurs from April to June (Figure 2), and onset timing is significantly correlated with air temperature in each month (Figure 10). Note the area with a significant relationship changes from lower latitudes in April to higher latitudes in May/June as snowmelt onset advances. Correlation analysis (using detrended series) shows that both July and August sea ice extent exhibit significant negative correlations with spring (April–May–June) air temperature ($r = -0.63$ for both months). Sea ice extent in other months is not significantly correlated with spring air temperature. This result suggests that spring air temperature anomalies are the main mechanism for significant correlations between melt onset on land and sea ice extent. Previous studies have shown that a meridional wind circulation pattern is the main driver for recent dramatic reductions in summer sea ice extent, which is also associated with the Arctic-wide spring warming [*Overland et al.*, 2008; *Overland and Wang*, 2010; *Wang et al.*, 2009].

4. Summary and Conclusions

[41] We present the first integrated pan-Arctic data set of melt onset date, produced by combining estimates derived from active and passive microwave satellite data using unique, previously published algorithms developed for the northern high-latitude land surface, ice caps, large lakes, and sea ice. This data set allows new insights into the major spatial and temporal patterns in melt onset and the associated geographic and topographic controls. It provides a unique data set for validating and improving simulations from regional or global climate models during the spring transition period when snow cover exerts the strongest

feedback on the climate system [*Déry and Brown*, 2007; *Flanner et al.*, 2011; *Groisman et al.*, 1994].

[42] In the terrestrial Arctic, tree fraction and latitude explain more than 60% of the variance in MMOD, with the former exerting a stronger influence on MMOD than the latter. On Arctic sea ice, the spatial distribution of MOD is patchy and the interannual variability is generally larger than on land. Melt did not reach the high elevations of some ice caps in the QEI in some cold summers, such as 2002 and 2004. Melt extent reached a maximum on the GrIS in 2002 during the most recent decade. During the 2000–2009 period, 2005/2004 had the earliest/latest MOD over the entire Arctic.

[43] About 58% of the terrestrial Arctic exhibits a positive relationship between MMOD and elevation, with a mean value of 24.5 m d^{-1}. Large mean vertical melt progression rates (50–90 m d^{-1}) are concentrated in the foothills of the mountains and at low elevations on the ice caps and GrIS. Low rates (<20 m d^{-1}) are found in areas with limited surface relief. However, some windswept environments, such as the North Slope of Alaska, exhibit significant negative relationships between MMOD and elevation. These regions cover 6% of the total land area and are in close agreement with the areas of significant negative relationship between spring SCD and elevation, which is due to wind scour of snow on exposed uplands with limited vegetation [*Brown et al.*, 2007; *Déry et al.*, 2004].

[44] Melt onset progresses fastest over land in areas without much change in land cover or elevation. The typical progression rate in these areas is 40–80 km d^{-1}. The mean horizontal melt progression rate decreases to less than 10 km d^{-1} in the mountainous areas, on ice caps, and in the boreal forest-tundra ecotones. Melt onset progresses very slowly in the marginal seas, probably because of wind-driven sea ice advection from the interior Arctic that inhibits the advance of melt near the ice edge [*Zhang et al.*, 2010]. Melt onset advances much more rapidly in the central Arctic, where the progression rate can exceed 100 km d^{-1}.

[45] Correlation analysis suggests that changes in MOD on sea ice have not played a significant role in recent reductions in summer sea ice extent. During the period 2000–2009, melt onset timing on sea ice is significantly correlated only with November sea ice extent. However, MOD on sea ice was significantly correlated with summer sea ice extent (June to September) during the previous decade (1990–1999). The lack of significant correlations between MOD on sea ice and summer sea ice extent during the most recent decade is probably due to thinner ice that is more vulnerable to other factors. MOD on land and July/August sea ice extent exhibit significant correlations with spring air temperature and with each other, suggesting that spring air temperature anomalies are the main mechanism driving significant correlations between melt onset on land and sea ice extent.

[46] Compared to satellite observations, the CGCM3-simulated MMOD shows good agreement over land areas but weaker agreement over sea ice, particularly in the central Arctic, where the simulated MMOD is later than the observed by about 2–3 weeks (Table 3). Delayed melt onset over sea ice is in agreement with findings of cold surface temperature bias in CGCM3 [*Chapman and Walsh*, 2007; *Karlsson and Svensson*, 2011]. The mean melt horizontal progression rates are overall lower from CGCM3 than from satellite data, especially over the boreal forest and the central Arctic sea ice.

[47] Through comparisons of the spatial and temporal variability and the mean horizontal progression rate in MMOD from satellite and CGCM3 data, we demonstrate that the integrated melt onset data set is well suited to evaluate climate model simulations. This metric could therefore be used to evaluate other models and help to diagnose issues with high-latitude snow and ice cover in present-day climate model simulations.

[48] **Acknowledgments.** This study was carried out as part of the International Polar Year project "Variability and Change in the Canadian Cryosphere," supported by the Government of Canada Program for the International Polar Year. The authors thank Warren Lee for providing the CGCM3 data, Mike Lazare and Ed Chan for helpful discussion about CGCM3 outputs, Diana Verseghy and Paul Bartlett for helpful discussion about snow simulations in CLASS, and Yi Luo for providing MODIS clear-sky composite images. The helpful comments from three anonymous referees are gratefully acknowledged.

References

Abdalati, W., and K. Steffen (1995), Passive microwave-derived snowmelt regions on the Greenland ice sheet, *Geophys. Res. Lett.*, *22*, 787–790, doi:10.1029/95GL00433.

Anderson, M. R., and S. D. Drobot (2001), Spatial and temporal variability in snowmelt onset over Arctic sea-ice, *Ann. Glaciol.*, *33*, 74–78, doi:10.3189/172756401781818284.

Barber, D. G., and S. V. Nghiem (1999), The role of snow on the thermal dependence of backscatter over sea ice, *J. Geophys. Res.*, *104*(C11), 25,789–25,803, doi:10.1029/1999JC900181.

Belchansky, G. I., D. C. Douglas, and N. G. Platonov (2004), Duration of the Arctic sea ice melt season: Regional and interannual variability, 1979–2001, *J. Clim.*, *17*, 67–80, doi:10.1175/1520-0442(2004)017<0067:DOTASI>2.0.CO;2.

Betts, A. K., P. Viterbo, A. Beljaars, H.-L. Pan, S.-Y. Hong, M. Goulden, and S. Wofsy (1998), Evaluation of land-surface interaction in ECMWF and NCEP/NCAR reanalysis models over grassland (FIFE) and boreal forest (BOREAS), *J. Geophys. Res.*, *103*(D18), 23,079–23,085, doi:10.1029/98JD02023.

Brown, R. D., and A. Frei (2007), Comment on "Evaluation of surface albedo and snow cover in AR4 coupled models" by A. Roesch, *J. Geophys. Res.*, *112*, D22102, doi:10.1029/2006JD008339.

Brown, R. D., and P. Mote (2009), The response of Northern Hemisphere snow cover to a changing climate, *J. Clim.*, *22*, 2124–2145, doi:10.1175/2008JCLI2665.1.

Brown, R., P. Bartlett, M. MacKay, and D. Verseghy (2006), Evaluation of snow cover in CLASS for SnowMIP, *Atmos. Ocean*, *44*(3), 223–238, doi:10.3137/ao.440302.

Brown, R. D., C. Derksen, and L. Wang (2007), Assessment of spring snow cover duration variability over northern Canada from satellite datasets, *Remote Sens. Environ.*, *111*, 367–381, doi:10.1016/j.rse.2006.09.035.

Cavalieri, D., C. Parkinson, P. Gloersen, and H. J. Zwally (1996), Sea Ice Concentrations from Nimbus-7 SMMR and DMSP SSM/I Passive Microwave Data, 1990–2009, http://nsidc.org/data/docs/daac/nsidc0051_gsfc_seaice.gd.html, Natl. Snow and Ice Data Cent., Boulder, Colo. [Updated annually.]

Chapman, W. L., and J. E. Walsh (2007), Simulations of Arctic temperature and pressure by global coupled models, *J. Clim.*, *20*, 609–632, doi:10.1175/JCLI4026.1.

Déry, S. J., and R. D. Brown (2007), Recent Northern Hemisphere snow cover extent trends and implications for the snow-albedo feedback, *Geophys. Res. Lett.*, *34*, L22504, doi:10.1029/2007GL031474.

Déry, S. J., W. T. Crow, M. Stieglitz, and E. F. Wood (2004), Modeling snow-cover heterogeneity over complex Arctic terrain for regional and global climate models, *J. Hydrometeorol.*, *5*(1), 33–48, doi:10.1175/1525-7541(2004)005<0033:MSHOCA>2.0.CO;2.

Drobot, S. D., and M. R. Anderson (2001a), An improved method for determining snowmelt onset dates over Arctic sea ice using scanning multichannel microwave radiometer and Special Sensor Microwave/Imager data, *J. Geophys. Res.*, *106*, 24,033–24,049, doi:10.1029/2000JD000171.

Drobot, S. D., and M. R. Anderson (2001b), Comparison of interannual snowmelt-onset dates with atmospheric conditions, *Ann. Glaciol.*, *33*, 79–84, doi:10.3189/172756401781818851.

Early, D. S., and D. G. Long (2001), Image reconstruction and enhanced resolution imaging from irregular samples, *IEEE Trans. Geosci. Remote Sens.*, *39*, 291–302, doi:10.1109/36.905237.

Fetterer, F., K. Knowles, W. Meier, and M. Savoie (2009), *Sea Ice Index, 1990–2009*, Natl. Snow and Ice Data Cent., Boulder, Colo.

Flanner, M. G., K. M. Shell, M. Barlage, D. K. Perovich, and M. A. Tschudi (2011), Radiative forcing and albedo feedback from the Northern Hemisphere cryosphere between 1979 and 2008, *Nat. Geosci.*, *4*, 151–155, doi:10.1038/ngeo1062.

Flato, G. M., and G. J. Boer (2001), Warming asymmetry in climate change simulations, *Geophys. Res. Lett.*, *28*, 195–198, doi:10.1029/2000GL012121.

Flato, G. M., and R. D. Brown (1996), Variability and climate sensitivity of landfast Arctic sea ice, *J. Geophys. Res.*, *101*, 25,767–25,777, doi:10.1029/96JC02431.

Frei, A., R. Brown, J. A. Miller, and D. A. Robinson (2005), Snow mass over North America: Observations and results from the second phase of the Atmospheric Model Intercomparison Project (AMIP-2), *J. Hydrometeorol.*, *6*, 681–695, doi:10.1175/JHM443.1.

Gardner, A. S., and M. Sharp (2007), Influence of the arctic circumpolar vortex on the mass balance of Canadian High Arctic glaciers, *J. Clim.*, *20*, 4586–4598, doi:10.1175/JCLI4268.1.

Goulden, M. L., et al. (1998), Sensitivity of boreal forest carbon balance to soil thaw, *Science*, *279*, 214–217, doi:10.1126/science.279.5348.214.

Graversen, R. G., T. Mauritsen, S. Drijfhout, M. Tjernström, and S. Mårtensson (2011), Warm winds from the Pacific caused extensive Arctic sea-ice melt in summer 2007, *Clim. Dyn.*, *36*, 2103–2112, doi:10.1007/s00382-010-0809-z.

Grenfell, T. C., and D. K. Perovich (2004), The seasonal and spatial evolution of albedo in a snow-ice-land-ocean environment, *J. Geophys. Res.*, *109*, C01001, doi:10.1029/2003JC001866.

Groisman, P. Y., T. R. Karl, and R. W. Knight (1994), Observed impact of snow cover on the heat balance and the rise of continental spring temperatures, *Science*, *263*, 198–200, doi:10.1126/science.263.5144.198.

Hansen, M., R. DeFries, J. R. Townshend, M. Carroll, C. Dimiceli, and R. Sohlberg (2006), *MODIS Vegetation Continuous Fields MOD44B, 2001 Percent Tree Cover*, Collection 4, http://www.glcf.umd.edu/data/vcf/, Univ. of Maryland, College Park, Md.

Howell, S. E. L., A. Tivy, J. J. Yackel, and R. K. Scharien (2006), Application of a SeaWinds/QuikSCAT sea ice melt algorithm for assessing melt dynamics in the Canadian Arctic Archipelago, *J. Geophys. Res.*, *111*, C07025, doi:10.1029/2005JC003193.

Howell, S. E. L., C. R. Duguay, and T. Markus (2009a), Sea ice conditions and melt season duration variability within the Canadian Arctic Archipelago: 1979–2008, *Geophys. Res. Lett.*, *36*, L10502, doi:10.1029/2009GL037681.

Howell, S. E. L., L. C. Brown, K. K. Kang, and C. R. Duguay (2009b), Monitoring lake ice phenology variability on Great Bear Lake and Great Slave Lake, Northwest Territories, Canada, from SeaWinds/QuikSCAT: 2000–2006, *Remote Sens. Environ.*, *113*(4), 816–834, doi:10.1016/j.rse.2008.12.007.

Kalnay, E., et al. (1996), The NCEP/NCAR 40-year reanalysis project, *Bull. Am. Meteorol. Soc.*, *77*, 437–471, doi:10.1175/1520-0477(1996)077<0437:TNYRP>2.0.CO;2.

Karlsson, J., and G. Svensson (2011), The simulation of Arctic clouds and their influence on the winter surface temperature in present-day climate in the CMIP3 multi-model dataset, *Clim. Dyn.*, *36*(3–4), 623–635, doi:10.1007/s00382-010-0758-6.

Koerner, R. M. (2005), Mass balance of glaciers in the Queen Elizabeth Islands, Nunavut, Canada, *Ann. Glaciol.*, *42*, 417–423, doi:10.3189/172756405781813122.

Lindsay, R. W., J. Zhang, A. Schweiger, M. Steele, and H. Stern (2009), Arctic Sea Ice Retreat in 2007 Follows Thinning Trend, *J. Clim.*, *22*, 165–176, doi:10.1175/2008JCLI2521.1.

Long, D. G., and B. R. Hicks (2005), *Standard BYU QuikSCAT/SeaWinds land/ice image products*, report, Brigham Young Univ., Provo, Utah.

Luo, Y., A. P. Trishchenko, and K. V. Khlopenkov (2008), Developing clear-sky, cloud and cloud shadow mask for producing clear-sky composites at 250-meter spatial resolution for the seven MODIS land bands over Canada and North America, *Remote Sens. Environ.*, *112*, 4167–4185, doi:10.1016/j.rse.2008.06.010.

Markus, T., J. C. Stroeve, and J. Miller (2009), Recent changes in Arctic sea ice melt onset, freeze-up, and melt season length, *J. Geophys. Res.*, *114*, C12024, doi:10.1029/2009JC005436.

Maslanik, J., and J. C. Stroeve (1990), DMSP SSM/I Daily Gridded Brightness Temperatures, 1990–2009, http://nsidc.org/data/nsidc-0001.html, Natl. Snow and Ice Data Cent., Boulder, Colo. [Updated 2011.]

Mote, T. L., and M. R. Anderson (1995), Variations in snowpack melt on the Greenland ice sheet based on passive-microwave measurements, *J. Glaciol.*, *41*, 51–60.

Myneni, R. B., C. D. Keeling, C. J. Tucker, G. Asrar, and R. R. Nemani (1997), Increased plant growth in the northern high latitudes from 1981 to 1991, *Nature*, *386*, 698–702, doi:10.1038/386698a0.

Nakicenovic, N., et al. (2000). *Special Report on Emissions Scenarios: A Special Report of Working Group III of the Intergovernmental Panel on Climate Change*, Cambridge Univ. Press, Cambridge, U.K., 599 pp. Available online at: http://www.grida.no/climate/ipcc/emission/index.htm

Nghiem, S. V., I. G. Rigor, D. K. Perovich, P. Clemente-Colon, J. W. Weatherly, and G. Neumann (2007), Rapid reduction of Arctic perennial sea ice, *Geophys. Res. Lett.*, *34*, L19504, doi:10.1029/2007GL031138.

Overland, J. E., and M. Wang (2010), Large-scale atmospheric circulation changes are associated with the recent loss of Arctic sea ice, *Tellus, Ser. A*, *62*, 1–9, doi:10.1111/j.1600-0870.2009.00421.x.

Overland, J. E., M. Wang, and S. Salo (2008), The recent Arctic warm period, *Tellus, Ser. A*, *60*, 589–597, doi:10.1111/j.1600-0870.2008.00327.x.

Perovich, D. K., B. Light, H. Eicken, K. F. Jones, K. Runciman, and S. V. Nghiem (2007a), Increasing solar heating of the Arctic Ocean and adjacent seas, 1979–2005: Attribution and role in the ice-albedo feedback, *Geophys. Res. Lett.*, *34*, L19505, doi:10.1029/2007GL031480.

Perovich, D. K., S. V. Nghiem, T. Markus, and A. Schweiger (2007b), Seasonal evolution and interannual variability of the local solar energy absorbed by the Arctic sea ice–ocean system, *J. Geophys. Res.*, *112*, C03005, doi:10.1029/2006JC003558.

Perovich, D. K., J. A. Richter-Menge, K. F. Jones, and B. Light (2008), Sunlight, water, and ice: Extreme Arctic sea ice melt during the summer of 2007, *Geophys. Res. Lett.*, *35*, L11501, doi:10.1029/2008GL034007.

Räisänen, J. (2008), Warmer climate: Less or more snow? *Clim. Dyn.*, *30*, 307–319, doi:10.1007/s00382-007-0289-y.

Randall, D. A., et al. (2007), Climate models and their evaluation, in *Climate Change 2007: The Physical Science Basis. Contribution of Working Group I to the Fourth Assessment Report of the Intergovernmental Panel on Climate Change*, edited by S. Solomon et al., pp. 589–662, Cambridge Univ. Press, Cambridge, U.K.

Rawlins, M., K. McDonald, S. Frolking, R. Lammers, M. Fahnestock, J. Kimball, and C. Vorosmarty (2005), Remote sensing of pan-Arctic snowpack thaw using the SeaWinds scatterometer, *J. Hydrol.*, *312*, 294–311, doi:10.1016/j.jhydrol.2004.12.018.

Roesch, A. (2006), Evaluation of surface albedo and snow cover in AR4 coupled climate models, *J. Geophys. Res.*, *111*, D15111, doi:10.1029/2005JD006473.

Scinocca, J. F., N. A. McFarlane, M. Lazare, J. Li, and D. Plummer (2008), Technical Note: The CCCma third generation AGCM and its extension into the middle atmosphere, *Atmos. Chem. Phys.*, *8*, 7055–7074, doi:10.5194/acp-8-7055-2008.

Screen, J. A., and I. Simmonds (2010), The central role of diminishing sea ice in recent Arctic temperature amplification, *Nature*, *464*, 1334–1337, doi:10.1038/nature09051.

Screen, J. A., and I. Simmonds (2011), Declining summer snowfall in the Arctic: Causes, impacts and feedbacks, *Clim. Dyn.*, doi:10.1007/s00382-011-1105-2.

Serreze, M. C., J. A. Maslanik, J. R. Key, R. F. Kokaly, and D. A. Robinson (1995), Diagnosis of the record minimum in Arctic sea ice area during 1990 and associated snow cover extremes, *Geophys. Res. Lett.*, *22*, 2183–2186, doi:10.1029/95GL02068.

Serreze, M. C., M. M. Holland, and J. Stroeve (2007), Perspectives on the Arctic's shrinking sea-ice cover, *Science*, *315*, 1533–1536, doi:10.1126/science.1139426.

Sharp, M., and L. Wang (2009), A five-year record of summer melt on Eurasian Arctic ice caps, *J. Clim.*, *22*, 133–145, doi:10.1175/2008JCLI2425.1.

Slater, A. G., et al. (2001), The representation of snow in land surface schemes: Results from PILPS 2(D), *J. Hydrometeorol.*, *2*, 7–25, doi:10.1175/1525-7541(2001)002<0007:TROSIL>2.0.CO;2.

Smith, D. M. (1998), Observation of perennial Arctic sea ice melt and freeze-up using passive microwave data, *J. Geophys. Res.*, *103*, 27,753–27,769, doi:10.1029/98JC02416.

Sorteberg, A., and B. Kvingedal (2006), Atmospheric forcing on Barents Sea ice (2006), *J. Clim.*, *19*(19), 4772–4784, doi:10.1175/JCLI3885.1.

Stroeve, J., T. Markus, W. Meier, and J. Miller (2006), Recent changes in the Arctic melt season, *Ann. Glaciol.*, *44*, 367–374, doi:10.3189/172756406781811583.

Stroeve, J., M. M. Holland, W. Meier, T. Scambos, and M. Serreze (2007), Arctic sea ice decline: Faster than forecast, *Geophys. Res. Lett.*, *34*, L09501, doi:10.1029/2007GL029703.

Takala, M., J. Pulliainen, S. J. Metsamaki, and J. Koskinen (2009), Detection of snowmelt using spaceborne microwave radiometer data in Eurasia from 1979 to 2007, *IEEE Trans. Geosci. Remote Sens.*, *47*, 2996–3007, doi:10.1109/TGRS.2009.2018442.

Trenberth, K. E., et al. (2007), Observations: Surface and atmospheric climate change, in *Climate Change 2007: The Physical Science Basis. Contribution of Working Group I to the Fourth Assessment Report of the Intergovernmental Panel on Climate Change*, edited by S. Solomon et al., pp. 235–336, Cambridge Univ. Press, Cambridge, U.K.

Ulaby, F. T., R. K. Moore, and A. Fung (1982), *Microwave Remote Sensing: Active and Passive, vol. II, Radar Remote Sensing and Surface Scattering and Emission Theory*, 609 pp., Addison-Wesley, Reading, Mass.

Ulaby, F. T., R. K. Moore, and A. Fung (1986), *Microwave Remote Sensing: Active and Passive, vol. III, Volume Scattering and Emission Theory, Advanced Systems and Applications*, 1100 pp., Artech House, Dedham, Mass.

Verseghy, D. (1991), CLASS—A Canadian land surface scheme for GCMs. I: Soil model, *Int. J. Climatol.*, *11*, 111–133, doi:10.1002/joc.3370110202.

Verseghy, D. L., N. A. McFarlane, and M. Lazare (1993), CLASS—A Canadian land surface scheme for GCMs. II: Vegetation model and coupled runs, *Int. J. Climatol.*, *13*, 347–370, doi:10.1002/joc.3370130402.

Wang, J., J. Zhang, E. Watanabe, M. Ikeda, K. Mizobata, J. E. Walsh, X. Bai, and B. Wu (2009), Is the Dipole Anomaly a major driver to record lows in Arctic summer sea ice extent?, *Geophys. Res. Lett.*, *36*, L05706, doi:10.1029/2008GL036706.

Wang, L., M. Sharp, B. Rivard, S. Marshall, and D. Burgess (2005), Melt season duration on Canadian Arctic ice caps, 2000–2004, *Geophys. Res. Lett.*, *32*, L19502, doi:10.1029/2005GL023962.

Wang, L., M. Sharp, B. Rivard, and K. Steffen (2007), Melt season duration and ice layer formation on the Greenland ice sheet, 2000–2004, *J. Geophys. Res.*, *112*, F04013, doi:10.1029/2007JF000760.

Wang, L., C. Derksen, and R. Brown (2008), Detection of Pan-Arctic terrestrial snowmelt from QuikSCAT, 2000–2005, *Remote Sens. Environ.*, *112*, 3794–3805, doi:10.1016/j.rse.2008.05.017.

Wolken, G. J., M. Sharp, and L. Wang (2009), Snow and ice facies variability and ice layer formation on Canadian Arctic ice caps, 1999–2005, *J. Geophys. Res.*, *114*, F03011, doi:10.1029/2008JF001173.

Zhang, J., R. Woodgate, and R. Moritz (2010), Sea ice response to atmospheric and oceanic forcing in the Bering Sea, *J. Phys. Oceanogr.*, *40*, 1729–1747, doi:10.1175/2010JPO4323.1.

Zhang, X., J. E. Walsh, J. Zhang, U. S. Bhatt, and M. Ikeda (2004), Climatology and interannual variability of Arctic cyclone activity, 1948–2002, *J. Clim.*, *17*, 2300–2317, doi:10.1175/1520-0442(2004)017<2300:CAIVOA>2.0.CO;2.

R. D. Brown, Ouranos Consortium on Regional Climatology and Adaptation to Climate Change, 19th Floor, West Tower, 550 Sherbrooke W., Montreal, QC H3A 1B9, Canada.

J. Cole, C. Derksen, S. E. L. Howell, and L. Wang, Climate Research Division, Atmospheric Science and Technology Directorate, Environment Canada, 4905 Dufferin St., Toronto, ON M3H 5T4, Canada. (Libo.Wang@ec.gc.ca)

T. Markus, Cryospheric Sciences Branch, NASA Goddard Space Flight Center, Greenbelt, MD 20771, USA.

M. J. Sharp, Department of Earth and Atmospheric Sciences, University of Alberta, 1-26 Earth Science Bldg., Edmonton, AB T6G 2E3, Canada.

G. J. Wolken, Alaska Division of Geological and Geophysical Surveys, 3354 College Rd., Fairbanks, AK 99709, USA.